Modelling the plastic deformation during high-temperature creep of a powder-metallurgy coarse-grained superalloy

Sofiane Terzi, Raphael Couturier, Laure Guétaz, Bernard Viguier

Modelling the plastic deformation during high-temperature creep of a powder-metallurgy coarse-grained superalloy

Sofiane Terzi [a], Raphael Couturier [a], Laure Guétaz [a], Bernard Viguier [b,*]

[a] *CEA Grenoble, DRT-LITEN-DTH, 38054 Grenoble Cedex 9, France*
[b] *CIRIMAT, ENSIACET-INP, 118 Route de Narbonne, 31077 Toulouse Cedex 4, France*

Abstract

The study of creep deformation in a coarse-grained Udimet 720 superalloy obtained by powder-metallurgy reveals a good resistance associated to a dislocational deformation mechanism. A model is proposed for simulating creep and tensile curves. This model is used to understand the effect of microstructural changes on the deformation mechanisms.

Keywords: Model; Creep; Dislocation density; Udimet 720; Powder-metallurgy

1. Introduction

The development of the next generation of nuclear power plants requires a new design of the structural parts such as turbine disks. For instance, the French high-temperature nuclear reactor project includes a very large turbine disk working in severe conditions. Udimet 720 superalloy is a potential candidate for fabricating such disks able to sustain creep at temperature ranging around 700 °C for very long time (maintenance periodicity of 60,000 h is attempted) [1]. For insuring the metallurgical homogeneity within so large pieces the powder-metallurgy (PM) processing appears as an encouraging route provided one can produce a structure with large austenitic grains. We briefly present in this paper the creep results obtained on such a large grain PM alloy. The second part of the paper presents the formalism of the physical model which is developed on the basis of dislocation density variations. Results of the model are shown in terms of creep and tensile curves and it is demonstrated that the model can help to understand the effect of microstructural changes on creep behaviour.

* Corresponding author. Tel.: +33 5 62 88 56 64; fax: +33 5 62 88 56 63.
E-mail address: Bernard.Viguier@ensiacet.fr (B. Viguier).

2. Experiment and results

We have used in the present study a low interstitial Udimet 720 alloy obtained by a PM route. A special procedure for consolidation and heat treatment has been designed in collaboration with Aubert and Duval [2]. The hot isostatic pressing (HIP) step is performed by uncoupling heating and pressurisation [3], then a multistep heat treatment is given to the alloy in order to insure the growth of grains and the precipitation of γ' reinforcing particles. The resulting microstructure reveals large grains (up to 80 μm) with grain boundaries (GBs) not correlated to the prior powder boundaries (PPBs). There are two different types of intragranular γ' precipitates: secondary γ' precipitates with a 650 nm edge cubic form and small spherical tertiary γ' precipitate with an average diameter of about 100 nm. Tensile and creep tests were performed on cylindrical specimens with 4 mm diameter and 20 mm gage length. Tensile tests demonstrated that the alloy produced in this way exhibits yield and strength behaviour comparable to those of cast and wrought (C&W) alloys [1]. Creep tests performed at 700 and 750 °C under stresses ranging form 350 to 750 MPa revealed typical three-stage creep behaviour with a good reproducibility. The strain to rupture obtained in the present creep tests is higher than for the previously tested PM alloy with fine grains [4] and the present alloy approaches the creep resistance of coarse-grained C&W materials [5]. Scanning electron microscopy (SEM) of crept specimens showed that damage occurs by intergranular cavitation. In PM materials, the

doi:10.1016/j.msea.2006.10.186

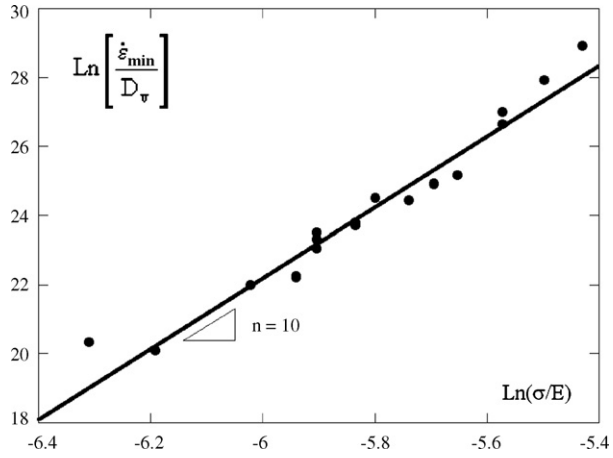

Fig. 1. Norton plot showing the evolution of strain rate normalised by the self-diffusion coefficient vs. stress normalised by Young's modulus, showing that a unique mechanism prevails in all the creep tests realised.

GBs contiguous with PPB precipitates are preferential sites for the formation of cavities [6]. The special HIP cycle and heat treatment that have been designed for producing the alloy result in much less PPB particles located in the GBs, thus reducing the number of cavitation sites. The improvement in creep resistance observed in the present alloy seems not to be only a consequence of less damage. The secondary creep rate is observed to be low and close to the creep rate observed in C&W alloys even at low stresses. A logarithmic plot of normalised secondary creep rate versus the normalised creep stress shows that a unique Norton coefficient ($n = 10$) prevails as shown in Fig. 1.

This observation indicates that a unique dislocational creep mechanism operates at different stresses, in contrast with finer grain size PM alloy 720 in which GB sliding controls the deformation at the lowest stresses and induces a higher creep rate [7]. Transmission electron microscopy (TEM) on crept specimens reveal many dislocation loops around the γ' particles and very few stacking faults in them, suggesting an Orowan mechanism for by-passing the precipitates. Those observations were taken into account for modelling the deformation of the alloy which is presented in Section 3.

3. Modelling

The plasticity of Udimet 720 alloy has been treated in the framework of models based on the evolution of dislocation densities, developed for fcc metals and alloys [8–10]. In the thermal-activation concept, the rate of shear strain $\dot{\gamma}$ is given by an Arrhenius function of the effective shear stress τ^* and activation volume V^* [see, e.g., ref. [11]]:

$$\dot{\gamma} = \dot{\gamma}_0 \exp\left[\frac{\tau^* V^*}{k_B T}\right] \tag{1}$$

where k_B is the Boltzmann constant and T is the absolute temperature. The pre-exponential terms include the density of mobile dislocations ρ_m

$$\dot{\gamma}_0 = \rho_m b^2 \nu_D \exp\left(-\frac{\Delta G_0}{k_B T}\right) \tag{2}$$

with b the magnitude of the Burgers vector of moving dislocations, ν_D the Debye frequency and ΔG_0 is the total free enthalpy for passing through local obstacles.

The effective stress is defined by $\tau^* = (\tau_a - \tau_\mu)$, where τ_a is applied resolved shear stress and τ_μ the internal stress connected to long range obstacles. This internal stress has been considered to be due to the interactions with dislocations (Taylor's law, with the total dislocation density ρ_t) and to the hardening precipitates through a constant term τ_p:

$$\tau_\mu = \alpha \mu b \sqrt{\rho_t} + \tau_p \tag{3}$$

in which μ is the shear modulus and α is a coefficient that represents the proper interaction mechanism (in the present calculation this coefficient was set to an "average" value: $\alpha = 0.3$ [12]).

During a creep test, since the applied stress is kept constant the strain is mainly governed by the evolution of the total dislocation density $\dot{\rho}_t$ which is expressed as the sum of the evolution of two dislocation populations: the mobile ($\dot{\rho}_m$) and immobile ($\dot{\rho}_i$) dislocation densities. The evolution of mobile and immobile dislocation densities can be written as:

$$\dot{\rho}_m = \dot{\rho}_m^p - \dot{\rho}_m^a - \dot{\rho}_m^i \quad \text{and} \quad \dot{\rho}_i = \dot{\rho}_i^p - \dot{\rho}_i^a \tag{4}$$

where the upper-script "p" means production, "a" for annihilation and finally "i" means immobilisation. The production of immobile dislocations is due to the immobilisation of moving ones ($\dot{\rho}_i^p = \dot{\rho}_i^m$) and it can be assumed that dislocation annihilation occurs through the reaction between a mobile and an immobile dislocation (which sets: $\dot{\rho}_m^a = \dot{\rho}_i^a$). The whole dislocation density evolution is thus governed by three terms: $\dot{\rho}_m^p$, $\dot{\rho}_m^a$, $\dot{\rho}_m^i$. If we further assume that the density of mobile dislocations is constant one can write: $\dot{\rho}_m^p = \dot{\rho}_m^a + \dot{\rho}_m^i$. Two terms still remain to be calculated: the annihilation and immobilisation terms. The immobilisation can be written as a function of a "mean free distance before immobilisation" Λ [10]:

$$\dot{\rho}_m^i = \frac{\dot{\gamma}}{\Lambda b}. \tag{5}$$

For the present case, it appears that the mobile dislocations can be locked by either other dislocations or precipitates, that is the "mean free distance before immobilisation" can be written:

$$\frac{1}{\Lambda} = \frac{1}{\Lambda_1} + \frac{1}{\Lambda_2} \tag{6}$$

with $\Lambda_1 = N_1/\sqrt{\rho_t}$ and $\Lambda_2 = N_2\langle D\rangle$, $\langle D\rangle$ is the mean distance between γ' precipitates (which was measured to be $\langle D\rangle = 100\,\text{nm}$), N_1 and N_2 represent the number of obstacles that can be by-passed before immobilisation.

The annihilation rate of mobile dislocations interacting with immobile ones is related to the recovery rate. Such relation can be written as [13–15]:

$$\dot{\rho}_m^a = K\left(\frac{\dot{\gamma}}{\dot{\gamma}_0}\right)^{-(1/n)} \frac{\dot{\gamma}}{b}\rho_i, \tag{7}$$

where the coefficients K and n are related to macroscopic hardening rate of the material. Since the mobile dislocation density

is only a small part of the total density, ρ_i can be approximated by ρ_t in Eq. (7). Finally, the evolution of the total dislocation density sums up to be $\dot{\rho}_t = \dot{\rho}_m + \dot{\rho}_i = \dot{\rho}_i = \dot{\rho}_m^i - \dot{\rho}_m^a$ and the whole plastic behaviour of the alloy obeys the system:

$$\begin{cases} \dot{\gamma} = \dot{\gamma}_0 \exp\left[\dfrac{(\tau_a - \alpha\mu b\sqrt{\rho_t} - \tau_p)V^*}{k_B T}\right] \\ \dot{\rho}_i = \dot{\rho}_t = \left(\dfrac{\sqrt{\rho_t}}{N_1} + \dfrac{1}{N_2\langle D\rangle}\right)\dfrac{\dot{\gamma}}{b} - K\left(\dfrac{\dot{\gamma}}{\dot{\gamma}_0}\right)^{-(1/n)}\rho_t\dfrac{\dot{\gamma}}{b} \end{cases} \quad (8)$$

Note that for the calculations, macroscopic stress σ and strain ε variables were used in order to compare directly to the experimental results. A Taylor constant $M = 3$, has been used accordingly to relate both sets of coordinates ($\varepsilon = \gamma/M$; $\sigma = M\tau$). All the calculations have been conducted for $T = 700\,^{\circ}\mathrm{C}$, the temperature at which we have the larger number of experimental results. For the calculation of creep tests the applied stress is a data and we calculate the strain rate (in the experimental frame the load is kept constant; we corrected the value of applied stress with the variation of specimen section assuming a constant volume). For the tensile testing, the total strain rate was imposed and the stress is calculated.

The effective activation volume which appears in Eq. (8) has been determined by means of repeated stress relaxation [16] during tensile tests. A value of $V^* = 62b^3$ corresponding roughly to the mean value obtained experimentally [5] led to satisfactory calculation results and was set constant. The remaining parameters that are adjusted to best fit the curves are thus:

- the pre-exponential strain rate $\dot{\varepsilon}_0 = \dot{\gamma}_0/M$;
- the stress due to the precipitates $\sigma_p = M{\cdot}\tau_p$;
- the mean free path before dislocation immobilisation through the numbers N_1 and N_2;
- the hardening coefficient K and n related to the dislocation annihilation.

As we have seen all these coefficients have a precise physical meaning and a numerical estimation, as well as a "reasonable" variation range could be defined which are shown in Table 1. The more precise values of these parameters have been numerically adjusted (using Sidolo software) to best fit the primary and secondary domains of experimental creep curves obtained at three different stress levels (750, 575 and 450 MPa). The results of this process are given in Fig. 2 and the resulting values of the six parameters are listed in Table 1.

Table 1
Fitting parameters used in the model, the estimated values served as the starting point for the fit, variations were allowed in the range indicated and the values obtained after the fit of three creep curves (see Fig. 2) are given

Parameter (units)	Estimate	Fitting range (min–max)	Fitted value
$\dot{\varepsilon}_0$ (s^{-1})	2×10^{-10}	10^{-10}–10^{-9}	1.9×10^{-10}
σ_p (MPa)	300	200–400	305
N_1	100	10–600	141
N_2	20	1–60	17
K (m)	10^{-8}	10^{-9}–10^{-6}	1.57×10^{-8}
n	8	6–10	6

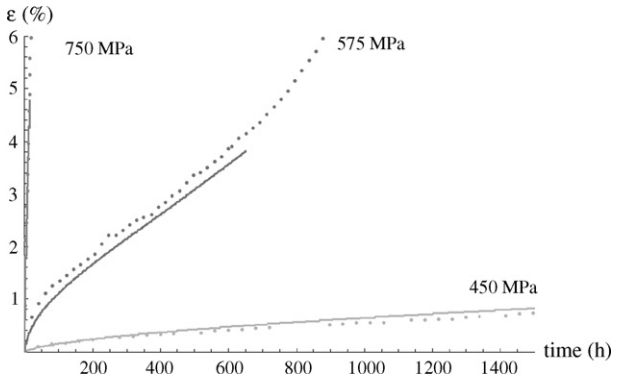

Fig. 2. Experimental creep curves (dots) which served to adjust the parameter of the model (full lines). The fit was performed up to the onset of tertiary creep regime as shown by the extension of the lines (the proposed model simulates the plastic deformation, not the damage).

One can see that all the values are well inside the ascribed range, keeping the physical meaning of those parameters. The same values were then used to calculate the creep curves for large range of stress (from 350 to 750 MPa) using Mathematica® software. The comparison between experimental points and calculated curves is shown in Fig. 3. One can notice the quite good agreement between calculated and experimental curves for most of the stress levels (only the creep test performed at 600 MPa exhibits a surprisingly lower creep rate than expected).

The same set of parameters has also been used to simulate successfully the tensile tests performed at 700 °C using different imposed strain rates as shown in Fig. 4. The agreement is convincing for the two lower strain rates (5×10^{-6} and $5 \times 10^{-4}\ s^{-1}$). In contrast, for the faster strain rate ($10^{-1}\ s^{-1}$) the final stress level is quite correctly obtained but yielding is poorly reproduced.

We have verified the ability of the model to reproduce the evolution of creep properties of the alloy when some metallurgical variables are changed. Some creep specimens have been heat treated with slight modifications (the cooling rate after the solutionning treatment was set to 30 K/min instead of the usual 60 K/min) resulting in a modification of the microstructure. This modification kept constant the overall γ' volume fraction, with a

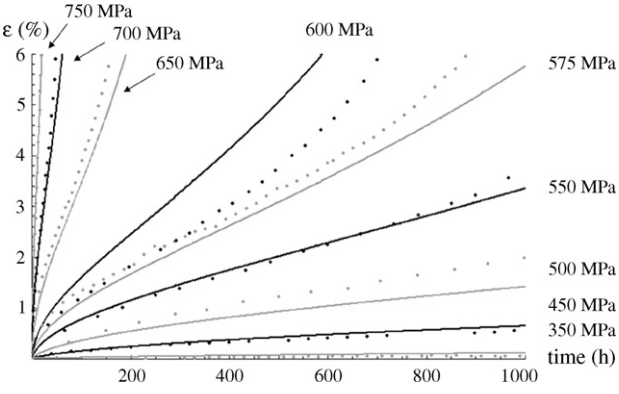

Fig. 3. Creep curves at various stress levels tested at 700 °C. The comparison between experimental (dots) and calculated (full lines) curves shows a fairly good agreement on the whole range of stresses.

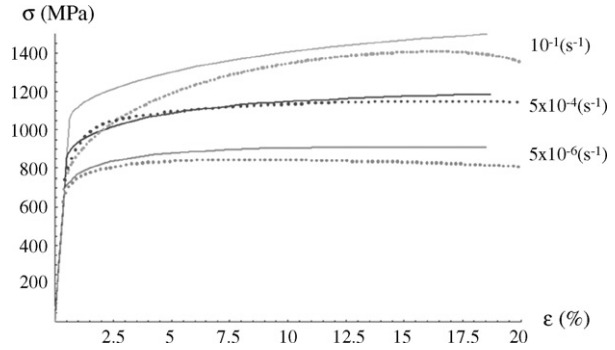

Fig. 4. The comparison between experimental (dots) and calculated (full lines) curves for tensile tests performed at 700 °C indicates that the model and the parameters obtained from creep allow to reproduce correctly tensile properties for the lower imposed strain rates.

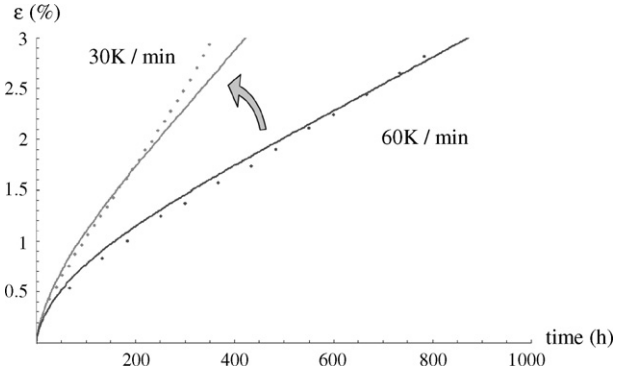

Fig. 5. Illustration of the modification of the creep curve due to a change in microstructure (resulting from a slower cooling rate). The experimental creep curves (dots) obtained at 700 °C under 550 MPa are well simulated by the model (full line). Between the simulation of the two curves only N_2 parameters is changed (see text).

coarsening of secondary γ' precipitation and fewer tertiary precipitates and led to an increase of the creep rate when tested at 700 °C as shown in Fig. 5(dots).

However, it is *a priori* not obvious to decide which is the precise mechanism that can explain this creep acceleration. The model could fit the new experimental curve only by changing the immobilisation parameter N_2. By fitting the experimental curve obtained at 550 MPa (full line in Fig. 5) the new value $N_2 = 32$ was determined. The new set of parameters could then be used to calculate the modified creep curves in the stress range 450–600 MPa. This demonstrates that the increase of the creep rate can be explained by the decrease of the dislocation storage on precipitates.

4. Conclusions

The results of creep tests performed on a coarse-grained PM alloy 720 are presented. It is shown that the good creep resistance obtained is related to a unique dislocational plastic deformation mechanism. A model is proposed based on the framework of thermal activation and governed by the evolution of dislocation densities. It is shown that the model can satisfactorily simulate creep and tensile curves and also allows to understand the role of microstructural changes on the creep behaviour.

References

[1] R. Couturier, H. Burlet, S. Terzi, S. Dubiez, L. Guétaz, G. Raisson, in: K.A. Green, T.M. Pollock, H. Harada, T.E. Howson, R.C. Reed, J.J. Schirra, S. Walston (Eds.), Superalloys 2004, TMS (The Minerals, Metals & Materials Society), Warrendale, PA, USA, 2004, pp. 351–359.
[2] G. Raisson, Private Communication, 2003.
[3] J. Davidson, US Patent 5,395,464 (1995).
[4] S. Dubiez-Le Goff, R. Couturier, L. Guétaz, H. Burlet, Mater. Sci. Eng. A 387–389 (2004) 599–603.
[5] S. Terzi, PhD Thesis, Institut National Polytechnique de Toulouse, France 2006.
[6] M. Norell, Ph.D. Thesis, Chamlers University of Technology, Göteborg, Sweden, 1996.
[7] S. Dubiez-Le Goff, Ph.D. Thesis, ENS Mines Paris, France, 2003.
[8] H. Mecking, K. Lücke, Scripta Metall. 4 (1970) 427–432.
[9] H. Mecking, U.F. Kocks, Acta Metall. 29 (1981) 1865–1875.
[10] E. Rauch, Habilitation à Diriger des Recherches, INP Grenoble, France, 1993.
[11] M. Cagnon, in: P. Groh, L.P. Kubin, J.L. Martfn (Eds.), Dislocations et deformation plastique, Les Editions de Physique, Yravals, 1979, pp. 53–66.
[12] B. Viguier, Mater. Sci. Eng. A 349 (2003) 132–135.
[13] U.F. Kocks, J. Eng. Mater. Technol. 98 (1976) 76–85.
[14] Y. Estrin, in: A. Krausz, K. Krausz (Eds.), Unified Constitutive Laws of Plastic Deformation, Academic Press, New York, 1996, pp. 69–106.
[15] M. Fivel, Ph.D. Thesis, INP Grenoble, France, 1997.
[16] P. Spätig, J. Bonneville, J.-L. Martin, Mater. Sci. Eng. A 167 (1993) 73–79.